Investigation of Superconducting Ti/Ti-Au/Au Tri-Layer Films With a Co-Sputtering Process for Transition-Edge Sensors

Investigation of Superconducting Ti/Ti-Au/Au Trilayer Films with a Co-sputtering Process for Transition-Edge Sensors

X. Xu, X. Sun, J. He, J. Chen, J. Li, M. Rajteri, H. Garrone, C. Pepe, H. Gao, X. Li, Y. Ouyang, and X. Wang

***Abstract*— The critical temperature (T_c) of superconducting Ti/Au bilayer films is crucial for the performance of transition-edge sensors. We use a co-sputtering technique to insert a Ti-Au mixture layer as an artificial diffusion layer between a superconducting Ti film and a normal Au bilayer. The Ti-Au mixture layers have different thicknesses and component ratios. The cross-section and element information of thin films was characterized by a high-resolution transmission electron microscopy (HRTEM) and energy dispersive X-ray spectroscopy (EDS). The variation of T_c is measured for a series of Ti/Ti-Au/Au films. T_c is related to both the thickness and Ti-Au ratio in the mixture layer. We attempt to model the T_c variation based on the Usadel theory with an equivalent thickness ratio.**

***Index Terms*—Ti/Au, Transition-Edge Sensor, superconductivity, co-sputtering, artificial diffusion, proximity effect**

I. Introduction

TRANSITION-Edge Sensors (TESs) fabricated by Ti/Au bilayer superconducting films are widely used for single photon detection [1]–[6] and X-ray detection [7]–[9]. Since the energy resolution of the TES strongly depends on the T_c [10], tunable and reliable T_c of the Ti/Au bilayer film is vital, as demonstrated by highest energy resolution of 67 meV at 0.8 eV [11] and huge potential for X-ray measurements with high energy resolution and multi-pixel instrumental applications [9] are obtainable.

This work was supported by National Key R&D Program of China (Grant No 2022YFF0608303), Young Scientists Fund of the National Natural Science Foundation of China (Grant No. 61901432). (Corresponding author: Jinjin Li and Xueshen Wang.)

X. Xu, J. Chen, J. Li, H. Gao, X. Li, Y. Ouyang, and X. Wang are with the National Institute of Metrology (NIM), 100029 Beijing, China (e-mail: xiaolong.xu@nim.ac.cn; chenjian@nim.ac.cn; jinjinli@nim.ac.cn; gaohf@nim.ac.cn; li-xu@nim.ac.cn; ouyangyanyan@nim.ac.cn; wangxs@nim.ac.cn).

X. Sun is with School of Information Engineering, Shenyang University of Chemical Technology,110142 Shenyang, China (e-mail: sxy17863904210@163.com)

J. He is with College of Physics, Sichuan University, 610064 Chengdu, China (e-mail: hejianhong@scu.edu.cn)

M. Rajteri is with the Istituto Nazionale di Ricerca Metrologica (INRiM), 10135 Torino, Italy (e-mail: m.rajteri@inrim.it).

H. Garrone, C. Pepe are with Department of Electronics and Telecommunications, Politecnico di Torino, 10129 Turin, Italy (e-mail: hobey.garrone@polito.it; carlo.pepe@polito.it)

Color versions of one or more of the figures in this paper are available online at http://ieeexplore.ieee.org.

For bilayer superconducting thin films, the T_c can be derived from the Usadel equation [12]. There are two ways to suppress the T_c: tuning the superconducting and normal metal layer thicknesses (or their ratio); tuning the interface transparency t. The thickness modification is a direct method to suppress the T_c obtained by decreasing the thickness of the Ti layer, increasing the thickness of the Au layer, i.e., increasing the ratio of Au/Ti. In comparison, the control of the interface transparency is more complicated. The t suffers from the baking process during the TES fabrication [13], aging, and thermal treatment in purpose [14], [15]. All the interface changes are essentially caused by the diffusion of Ti and Au atom through interface to form an Au-Ti mixed layer.

In this paper, an artificial diffusion layer is fabricated by co-sputtering Ti and Au. The establishment of the artificial diffusion structure and the effect on the T_c are demonstrated. Three series of sample for different diffusion depth and different Ti/Au diffusion concentrations are achieved. The multilayer film structures and the T_c are characterized. The diffusion model can be modeled by t from Usadel theory.

II. Experimental Details

A. Deposition of Ti/Ti-Au/Au Trilayer Films

Si substrates are used for the film deposition. The substrates are cleaned with acetone, isopropanol, deionized water, and then dried with N_2. The superconducting Ti/Ti-Au/Au trilayer films are deposited on the substrate in a Kurt J. Lesker cluster magnetron sputtering system with a base pressure of ~10^{-7} Pa. A Ti target (99.995 at. %) and an Au target (99.99 at. %) are used as the sputtering sources. The substrate is kept at 20 °C by a water-cooling system during the deposition process and rotates at 20 rpm to obtain the uniformity film. The sputtering pressure is 0.4 Pa. For the pure metal layer deposition, the sputtering power of Ti (P_{Ti}) is fixed at 300 W and that of Au (P_{Au}) is fixed at 200 W. For the intermediate Ti-Au mixture layer, P_{Au} is adjusted to 50 W, 75 W and 100 W while P_{Ti} is constant at 300 W during the co-sputtering process to prepare three series of films as shown in Fig. 1.

The total thickness of the Ti/Ti-Au/Au trilayer films is fixed at 130 nm. The deposition rate of Ti (300 W) and Au

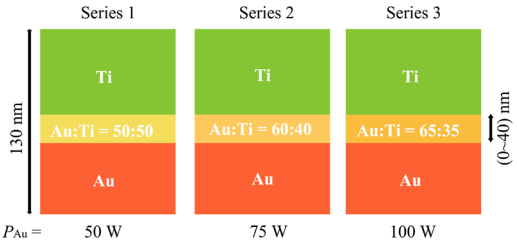

Fig. 1. Illustration of a series of Ti/Ti-Au/Au trilayer films.

(200 W) is 0.26 nm/s and 0.75 nm/s, respectively. To prevent a systematic T_c variation of the Ti film as a function of the sputtering target [16], all the samples are deposited using the same Ti target. The thickness of the layers is controlled by the deposition rate in the sputter process. The uncertainty component from the film thickness is 0.6% from the thin film deposition process and 4% from the uniformity of the film thickness. The thickness of intermediate layer increases from 0 to 40 nm, while the thicknesses of Ti and Au layers are accordingly reduced. The layer structures are summarized in Table. 1. The NIM-0 is the bilayer Ti (70 nm)/Au (60 nm) film, and NIM-1 to NIM-12 are the Ti/Ti-Au/Au trilayer films with different atom ratio $R_{Au\text{-}Ti}$ (atom%), 50:50 (NIM-1 to NIM-4), 60:40 (NIM-5 to NIM-8) and 65:35 (NIM-9 to NIM-12).

TABLE I
LAYER STRUCTURE OF 3 SERIES TI/TI-AU/AU TRILAYER FILMS

Sample	Thickness/nm			P_{Au}/W[a]	$R_{Au\text{-}Ti}$ (atom%)[b]
	Ti	Ti-Au	Au		
NIM-0	70	0	60		
NIM-1	63	14	53	50	50: 50
NIM-2	60	20	50		
NIM-3	57	26	47		
NIM-4	50	40	40		
NIM-5	63	14	53	75	60: 40
NIM-6	60	20	50		
NIM-7	57	26	47		
NIM-8	50	40	40		
NIM-9	63	14	53	100	65: 35
NIM-10	60	20	50		
NIM-11	57	26	47		
NIM-12	50	40	40		

[a] P_{Au}: The power of the Au target for the co-sputtering of the Ti-Au layer, the power of the Ti target is fixed at 300 W.
[b] $R_{Au\text{-}Ti}$: Atomic ratio of Au/Ti in the Ti-Au co-sputtering layer

B. Characterization of Ti/Ti-Au/Au Films

The cross-section of the Ti/Ti-Au/Au films is characterized with a high-resolution transmission electron microscope (HRTEM，Thermo Scientific Talos F200). The samples are prepared with a focused ion beam (FIB) technique in a dual beam SEM/FIB system (Helios 5UC). A Pt layer is deposited on the surface in order to protect the trilayer structure during the ion beam milling process. The film thickness is measured with a step profile (Bruker DektakXT). The uncertainty component for the film thickness is 0.5% from the step profile. An energy dispersive X-ray spectroscopy (EDS) is used to obtain the element information of every layer. The resistivity of trilayer films is mapped at room temperature by a resistivity mapper (CDE ResMap 178) [17] with a 4-wire method. 49 points are measured in the scale of 2-inch wafer with the probe

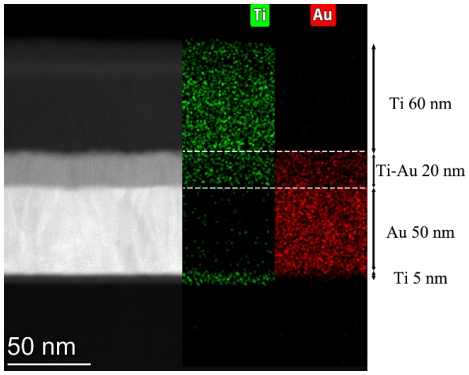

Fig. 2. The element distribution at the cross-section of the NIM-6 sample Ti (60 nm) /Ti-Au (20 nm) /Au (50 nm) trilayer film on a silicon substrate with a protective Pt layer coated.

structure of this instrument. The uncertainty of resistivity measurement is around 0.1%. The film was cut into 1 mm × 5 mm samples and wire bonded with Al wire, then it loaded into the Oxford dry dilution refrigerator (DR, Triton 200). The resistance of the films is measured with an excitation current of 1 μA by 4-wire method during the temperature increasing process to eliminate the effects of hysteresis. In our experience, I_c of our TES is around 500 μA (active area: 20 μm ×20 μm and ~100 nm thick) at 100 mK, therefore 1 μA is far below the I_c.

III. RESULTS AND DISCUSSION

A. Morphology of the Ti/Ti-Au/Au Films

Fig. 2 shows the HRTEM image of the NIM-6 sample Ti (60 nm)/Ti-Au (20 nm)/Au (50 nm). The 5 nm Ti is the adhesion layer for the Au deposition. The trilayer structure is well defined and the interfaces are clear. The element distribution is tagged with various colors. A small amount of Ti appears in the bottom Au layer due to the FIB milling process.

We also tried films in the flipped film ordering, where an Au layer was deposited on top of a thick bottom Ti layer to prepare Ti/Au bilayer thin film for TES. However, such films showed a weaker suppression of T_c, possibly due to the oxidation of the Ti surface before the Au deposition. In the current ordering of Ti/Ti-Au/Au, a deep oxidation of the top Ti layer can be avoided because a multilayer optical resonant cavity will be deposited on the TES.

B. Electrical Property

The resistivity ρ of the trilayer films is strongly correlated with the thickness of the co-sputtering Ti-Au layer as shown in Fig.3. The ρ increases when the thickness of the Ti-Au layer increases and Au layer decreases. The variation trend and amplitude of the resistivity can be used to evaluate the Ti-Au mixture degree of the Ti/Ti-Au/Au films.

The resistivity of trilayer films sightly increases as the atomic ratio of Au/Ti ($R_{\text{Au-Ti}}$) is larger. The initial Ti/Au bilayer film (NIM-0) shows the lowest ρ (107 nΩ·m), and NIM-12, the one with the thickest Ti-Au interlayer, shows the highest one (193 nΩ·m). Uncertainty of resistivity is less than 4.1% considering the contribution of the film thickness and resistivity measurement. The increasement of the resistivity with high $R_{\text{Au-Ti}}$ is similar to the results of PdAu alloy reported by Hall et al. [18]. The Au atom enhances the disorder effect of the co-sputtering layer.

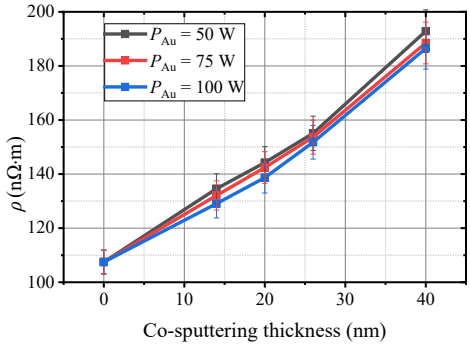

Fig. 3. Resistivity ρ vs. co-sputtering thickness of Ti-Au layer in trilayer thin films with different $R_{\text{Au-Ti}}$ of Ti-Au interlayer.

C. *Cryogenic Property*

The T_cs of the three series of films are shown in Fig. 4. The curves of resistance are measured after the temperature is stable for 15 minutes. The cryogenic system was calibrated with a ^{60}Co primary thermometer. Therefore, the error bar of temperature is less than 0.4%. The normal resistances of NIM-1 and NIM-2 are identical due to the geometric issue during the 4-wire wire bond. The Au film has suppressed the T_c of the Ti films via the proximity effect [19]. The thickness of the Ti-Au mixture layer obviously affects the T_c of the trilayer films. The T_c decreases as the thickness increases. The T_c of NIM-0, with the initial structure, is 311 mK, showing the weakest proximity effect among all samples. Inversely, the T_c of NIM-4 is 59 mK showing more intense proximity effect. The T_c also decreases by increasing $R_{\text{Au-Ti}}$ in the co-sputtering layer, which indicates that the gold component at the interface shows a significant T_c suppression effect. The T_c of NIM-10 reaches 54 mK, while the one of NIM-2, which has the same structure and a Ti-rich interlayer, is 216 mK. The too large thickness of the interlayer and too high $R_{\text{Au-Ti}}$ have induced the excessive suppression of the T_c. The T_c of NIM-8, NIM-11 and NIM-12 is below 15 mK (the base temperature of our dilution refrigerator).

An equivalent thickness model is proposed to analyze the effect of the interlayer. The thickness of the Ti and Au is equivalently determined according to Ti-Au atom ratio and added to the upper Ti layer and bottom Au layer, as shown in Fig.5. The bottom 5 nm Ti is the adhesion layer for the Au deposition, and is not superconducting. The thickness ratio of this layer to the Au layer and Ti-Au mixture layer is small, and

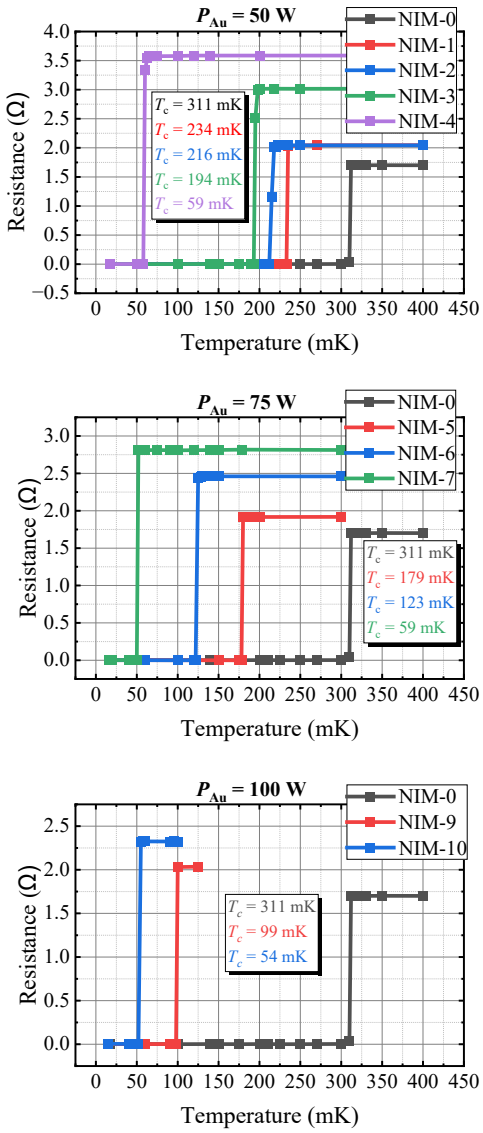

Fig. 4. The T_c of the Ti/Au and Ti/Ti-Au/Au films. (The error bars are smaller than the markers.)

will have a small effect on the modulation of the critical temperature of the upper Ti layer. So, this Ti layer is not considered for the following calculation. The equivalent thickness of the samples and corresponding T_c are summarized in Table II.

The T_c of the films is plotted as a function of the equivalent thickness ratio of Au-Ti in Fig.6. For the normal bilayer superconducting thin film, the high Au-Ti ratio will induce a

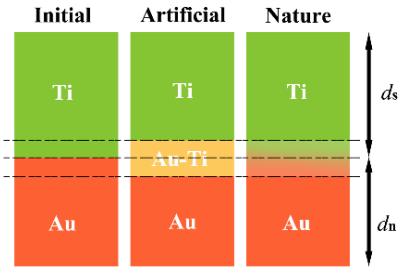

Fig. 5. Illustration of the equivalent thickness d_s and d_n.

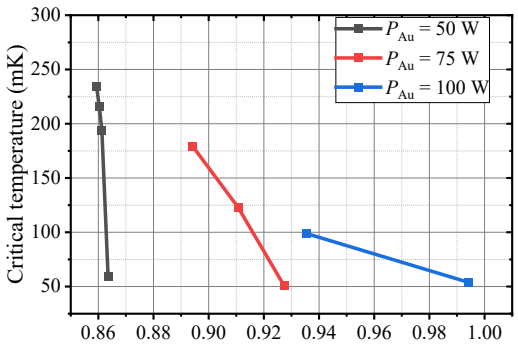

Fig. 6. Equivalent thickness ratio of Au-Ti in the trilayer films *vs.* T_c. (The error bars are smaller than the markers.)

lower T_c. For the $R_{Au\text{-}Ti}$ 50:50, the equivalent thickness is nearly the same, and the T_c decreases sharply with the Ti-Au mixture thickness, which is consistent with the diffusion effect induced by the thermal treatment [13], [14]. As the $R_{Au\text{-}Ti}$ increases from 60:40 to 65:35, the equivalent thickness ratios d_n/d_s are also increasing with the Ti-Au mixture thickness. This will make the T_c changes in large extent.

The relative change of the critical temperature $\Delta T_c/T_c$ compared to the initial structure is defined as:

$$\frac{\Delta T_c}{T_c} = \frac{T_{c\mathrm{NIM-0}} - T_{c\mathrm{NIM-x}}}{T_{c\mathrm{NIM-0}}} \quad (1)$$

Fig.7 shows the natural logarithm of $\Delta T_c/T_c$ *vs.* the inverse of Ti-Au mixture thickness. We learn from the concept of diffusion concentration and resistivity change from semiconductor science and try to explain the diffusion thickness relative to T_c change. [20] The slope of the linear fitting curve indicates the different degrees of T_c suppression effect. From the slope, the $R_{Au\text{-}Ti}$ decrease while the slope becomes steep. The T_c suppression effect of $R_{Au\text{-}Ti}$ is weaker than that caused by the diffusion thickness.

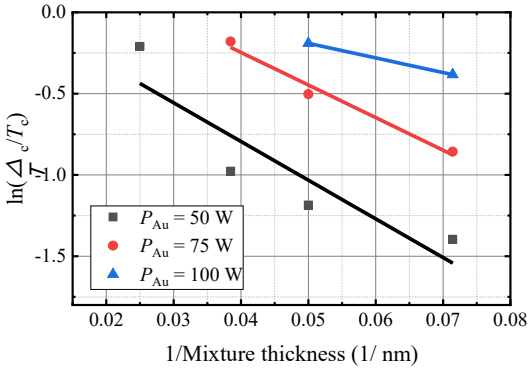

Fig. 7. The natural logarithm of normalized $\Delta T_c/T_c$ vs. the inverse of the mixture thickness.

D. *Diffusion mechanism of Ti/Au films*

In the NIM-0 Ti/Au layer, the Ti and Au atoms diffuse at the interface as illustrated in Fig. 5. To explain the T_c degradation in Ti/Au bilayers with an artificial Ti-Au mixture layer, we treat the entire Ti-Au mixture layer as an interface of the Ti/Au bilayer structure and use the Usadel theory. The Usadel theory is regarded a suitable framework for our study because it describes the behavior of superconducting structures in the diffusive limit [12].

TABLE II
EQUIVALENT THICKNESS OF AU, TI AND RELATIVE PARAMETERS FOR USADEL THEORY

Sample	Mixture thickness /nm	Equivalent thickness /nm		T_c/mK	t
		d_n	d_s		
NIM-0	0	60.0	70.0	311	0.8
NIM-1	14	60.1	69.9	234	6.6
NIM-2	20	60.1	69.9	216	12
NIM-3	26	60.2	69.8	194	26
NIM-4	40	60.2	69.8	59	2.0×10^5
NIM-5	14	61.4	68.6	179	34
NIM-6	20	62.0	68.0	123	460
NIM-7	26	62.5	67.5	51	1.6×10^5
NIM-8	40	63.9	66.1	-	-
NIM-9	14	62.2	66.5	99	1.6×10^3
NIM-10	20	63.1	63.5	54	3.4×10^4
NIM-11	26	64.0	60.5	-	-
NIM-12	40	66.2	53.5	-	-

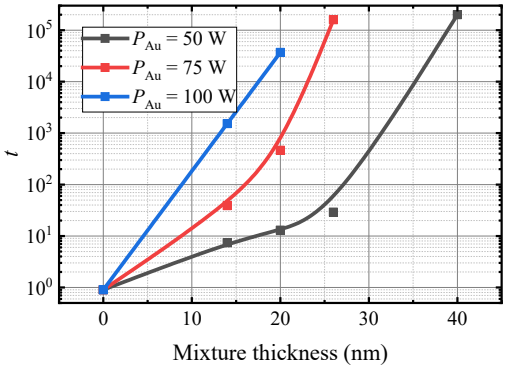

Fig. 8. Interference parameter t vs. mixture thickness in thin film.

In the Usadel theory, the following equations are used to predict T_c of a superconducting Ti/Au bilayer film [12]:

$$T_c = T_{c0}\left[\frac{d_s}{d_0}\frac{1}{1.13\left(1+\frac{1}{\beta}\right)}\frac{1}{t}\right]^{\beta} \quad (2)$$

$$\frac{1}{d_0} = \frac{\pi}{2}kT_{c0}\lambda_F^2 n_s \quad (3)$$

$$\beta = \frac{d_n n_n}{d_s n_s} \quad (4)$$

d_n and d_s are the equivalent thicknesses of the Au and Ti. n_n and n_s are the density of states, in our case n_n=1.07×10^{22} states/(eV·cm^3) [21], n_s=6.80×10^{22} states/(eV·cm^3) [22]. T_{c0}=550 mK is the T_c of the pure Ti film [23]. λ_F = 0.524 nm [21] is the Fermi wavelength of Au. k is the Boltzmann constant. t is the unitless parameter that describes the transmission through the interface of the bilayer film. The interface transparency t of the three series of films is calculated using the equation (2) and shown in Table. 2. Fig. 8 shows t as the func-

tion of mixture thickness and $R_{\text{Au-Ti}}$. The t values are calculated from the equation (2 to 4), we put those values in Table II and plot the curve in this figure. The interface transparency t increases with the mixture thickness. For the "clean" metals and their interface, t has a value of order one [12], [21]. In our case, we create a Ti-Au mixture layer at the Ti/Au interface, which makes the interface "dirty". The thickness of the Ti-Au mixture layer is larger than that generated by the diffusion process [13]. The condition of the artificial mixture layer and natural diffusion layer is different. This may be the reason why the t of NIM-4 reaches 2.0×10^5, more than five orders of magnitude larger comparing to the initial value 0.8 of NIM-0. For the same mixture thickness, the t of higher $R_{\text{Au-Ti}}$ shows nearly one order of magnitude larger than that of low $R_{\text{Au-Ti}}$, which is due to the Au-rich component in the diffusion zone. High $R_{\text{Au-Ti}}$ realizes a better T_c suppression effect.

IV. Conclusion

An artificial Ti-Au co-sputtering layer is used to modulate the T_c of Ti/Au superconducting films. The Ti-Au interlayer is considered as the diffusion zone of Ti and Au atom through the Ti-Au interface. The thickness of interlayer is regarded as the mixture thickness with different Au/Ti atom ratio. The T_c of Ti/Ti-Au/Au films are modulated dramatically with the Ti-Au interlayer. A Ti-Au diffusion and equivalent thickness model is established to link the natural diffusion with these artificial structures. In the frame of the Usadel theory, the interface transparency parameter t which indicates the extent of the proximity effect has shown great changes for different thickness and $R_{\text{Au-Ti.}}$

Acknowledgment

The authors would like to thank Mrs Qing Zhong at NIM for the helpful discussions.

References

[1] T. Konno, S. Takasu, K. Hattori, and D. Fukuda, "Development of an Optical Transition-Edge Sensor Array," *J. Low Temp. Phys.*, vol. 199, no. 1–2, pp. 27–33, 2020.

[2] X. Xu *et al.*, "Investigation of Ti/Au Transition-Edge Sensors for Single-Photon Detection," *J. Low Temp. Phys.*, vol. 209, no. 3–4, pp. 372–378, Nov. 2022.

[3] K. Hattori, R. Kobayashi, T. Numata, S. Inoue, and D. Fukuda, "Complex Impedance of Fast Optical Transition Edge Sensors up to 30 MHz," *J. Low Temp. Phys.*, vol. 193, no. 3–4, pp. 217–224, Nov. 2018.

[4] L. Lolli, E. Taralli, C. Portesi, D. Alberto, M. Rajteri, and E. Monticone, "Ti/Au transition-edge sensors coupled to single mode optical fibers aligned by Si V-groove," *IEEE Trans. Appl. Supercond.*, vol. 21, no. 3 PART 1, pp. 215–218, 2011.

[5] L. Lolli, E. Taralli, and M. Rajteri, "Ti/Au TES to Discriminate Single Photons," *J. Low Temp. Phys.*, vol. 167, no. 5–6, pp. 803–808, Jun. 2012.

[6] C. Portesi, E. Taralli, R. Rocci, M. Rajteri, and E. Monticone, "Fabrication of Au/Ti TESs for optical photon counting," *J. Low Temp. Phys.*, vol. 151, no. 1-2 PART 1, pp. 261–265, 2008.

[7] E. Taralli *et al.*, "AC/DC Characterization of a Ti/Au TES with Au/Bi Absorber for X-ray Detection," *J. Low Temp. Phys.*, vol. 199, no. 1–2, pp. 102–109, 2020.

[8] G. Wang *et al.*, "Developing x-ray microcalorimeters based on TiAu TES for HUBS," in *Space Telescopes and Instrumentation 2020: Ultraviolet to Gamma Ray*, 2020, no. December 2020, p. 224.

[9] K. Nagayoshi *et al.*, "Development of a Ti/Au TES Microcalorimeter Array as a Backup Sensor for the Athena/X-IFU Instrument," *J. Low Temp. Phys.*, vol. 199, no. 3–4, pp. 943–948, 2020.

[10] L. Lolli, E. Taralli, C. Portesi, E. Monticone, and M. Rajteri, "High intrinsic energy resolution photon number resolving detectors," *Appl. Phys. Lett.*, vol. 103, no. 4, p. 041107, Jul. 2013.

[11] K. Hattori, T. Konno, Y. Miura, S. Takasu, and D. Fukuda, "An optical transition-edge sensor with high energy resolution," *Supercond. Sci. Technol.*, vol. 35, no. 9, p. 095002, Sep. 2022.

[12] J. M. Martinis, G. . Hilton, K. . Irwin, and D. . Wollman, "Calculation of TC in a normal-superconductor bilayer using the microscopic-based Usadel theory," *Nucl. Instruments Methods Phys. Res. Sect. A Accel. Spectrometers, Detect. Assoc. Equip.*, vol. 444, no. 1–2, pp. 23–27, Apr. 2000.

[13] N. J. Van Der Heijden, P. Khosropanah, J. Van Der Kuur, and M. L. Ridder, "Diffusion behaviour in superconducting Ti/Au bilayers for SAFARI TES detectors," *J. Low Temp. Phys.*, vol. 176, no. 3–4, pp. 370–375, 2014.

[14] X. Xu *et al.*, "Influence of the Interface Composition to the Superconductivity of Ti/PdAu Films," *Nanomaterials*, vol. 11, no. 1, p. 39, Dec. 2020.

[15] B. Siri *et al.*, "Impact of annealing on TC and structure of titanium thin films," *IEEE Trans. Appl. Supercond.*, vol. 31, no. 5, 2021.

[16] F. W. Carter *et al.*, "Tuning SPT-3G Transition-Edge-Sensor Electrical Properties with a Four-Layer Ti–Au–Ti–Au Thin-Film Stack," *J. Low Temp. Phys.*, vol. 193, no. 5–6, pp. 695–702, 2018.

[17] "CDE Resmap 178 product information." [Online]. Available: https://cde-resmap.com/up-to-8-resmap-178/.

[18] P. M. Hall, J. M. Morabito, and J. M. Poate, "Diffusion mechanisms in the Pd/Au thin film system and the correlation of resistivity changes with Auger electron spectroscopy and Rutherford backscattering profiles," *Thin Solid Films*, vol. 33, no. 1, pp. 107–134, Mar. 1976.

[19] M. Parra-Borderias *et al.*, "Characterization of a Mo/Au thermometer for ATHENA," *IEEE Trans. Appl. Supercond.*, vol. 23, no. 3, 2013.

[20] D. B. Cuttriss, "Relation between surface concentration and average conductivity in diffused layers in germanium," *Bell Syst. Tech. J.*, vol. 40, no. 2, pp. 509–521, 1961.

[21] J. C. Weber *et al.*, "Development of a transition-edge sensor bilayer process providing new modalities for critical temperature control," *Supercond. Sci. Technol.*, vol. 33, no. 11, 2020.

[22] P. Blaha, K. Schwarz, and P. H. Dederichs, "Electronic structure of hcp metals," *Phys. Rev. B*, vol. 38, no. 14, pp. 9368–9374, Nov. 1988.

[23] X. Xu *et al.*, "Investigation of Superconducting Titanium films for Transition Edge Sensors," in *2020 Conference on Precision Electromagnetic Measurements (CPEM)*, 2020, pp. 1–2.